International Journal of Mechanical Sciences 301 (2025) 110445

Contents lists available at ScienceDirect

International Journal of Mechanical Sciences

journal homepage: www.elsevier.com/locate/ijmecsci

Experimental analysis of rate-dependent toughness of 3D-printed soft interface composites

Suhib Abu-Qbeitah [a,b,*], Olga Petrenko [a], Konstantin Y. Volokh [c], Stephan Rudykh [a]

[a] School of Mathematical & Statistical Sciences, University of Galway, Galway H91 TK33, Ireland
[b] School of Mechanical Engineering, Tel Aviv University, Tel Aviv, 6997801, Israel
[c] Faculty of Civil and Environmental Engineering, Technion - Israel Institute of Technology, Haifa 32000, Israel

ARTICLE INFO

Keywords:
Fracture mechanics
Experimental mechanics
Additive manufacturing
Nacre-like composites
Rate-dependent fracture
Inclusion failure

ABSTRACT

The hierarchical structure of biological nacre has long inspired the design of tough, damage-tolerant synthetic composites for advanced engineering applications. In this study, nacre-inspired composites were fabricated via additive manufacturing, embedding rigid inclusions within a soft polymer matrix, and systematically tested to complete fracture. We proposed innovative geometric designs and benchmarked them against the nacre-like architecture, validating experimental outcomes using the material-sink (MS) fracture modeling framework. This work is the first to reveal the rate-dependent fracture pathways in nacre-like composites across a wide spectrum of loading rates – from quasi-static to dynamic – and to document the novel emergence of inclusion fracture as a dominant failure mode at high strain rates. Moreover, the nacre-like design demonstrated exceptional mechanical performance – outperforming alternative architectures by nearly an order of magnitude in work of fracture – due to its unique, multi-stage fracture mechanism that delays and distributes damage progressively. These findings offer critical new insights into the interplay between architectural design and strain-rate effects, providing unprecedented guidance for optimizing nacre-inspired composites for dynamic, load-bearing applications.

1. Introduction

Biological composites such as nacre have long served as a source of inspiration for developing synthetic materials with exceptional mechanical properties. These natural materials combine high strength and toughness – two properties typically considered mutually exclusive in engineering materials – through hierarchical organization and strategic use of dissimilar constituents. This study builds on that foundation by investigating nacre-inspired composites fabricated via additive manufacturing. We conduct experimental testing to assess performance under both quasi-static and dynamic loading, focusing on failure energy and identifying key design principles..

In many synthetic materials, strength and toughness are typically considered mutually exclusive properties [1,2]. Conversely, over countless years of natural evolution, nature-made structures continually refine themselves, exhibiting remarkable mechanical properties. This serves as a source of inspiration for designers, propelling advancements in the design of synthetic structures in recent times [3–11]. Noticeably, certain naturally occurring structures exhibit remarkable mechanical performance by simultaneously possessing high strength and exceptional fracture resistance (resilience). The latter property can be assessed by the energy dissipated during the fracture process, often referred to as failure energy [12–18]. Notably, nacre, also known as mother-of-pearl, represents a nanocomposite material forming the interior layer of mollusk shells and is also used in the production of pearls. In essence, pearls are composed of the exact same material as the surrounding shell—namely, nacre [19].

These nature-inspired composites have high potential applications in various fields owing to their various functionalities [20–24], for instance, electrical conductivity [25,26], gas barriers [27], thermal stability and flame retardancy [28,29], underwater superoleophobic properties [30], and complete biodegradability [31], amongst others [32–34]. Duminy et al. [35] investigated the damage in nacre-inspired alumina. Their study involved physical experiments as well as modeling and concluded that the staggered arrangement prompts interaction with crack at the micro-level.

Predominantly, nacre is created from approximately 95% by volume of calcium carbonate ($CaCO_3$) - Fig. 1, which is a brittle material; nonetheless, it demonstrates notable fracture toughness [36–42]. These aragonite (calcium carbonate) inclusions have a diameter and thickness of 5–10 μ m and 0.3 – 0.5 μ m, respectively [43]. No synthetic material

* Corresponding author at: School of Mathematical & Statistical Sciences, University of Galway, Galway H91 TK33, Ireland.
E-mail address: suhib.abuqbeitah@universityofgalway.ie (S. Abu-Qbeitah).

https://doi.org/10.1016/j.ijmecsci.2025.110445
Received 15 March 2025; Received in revised form 27 May 2025; Accepted 30 May 2025
Available online 18 June 2025

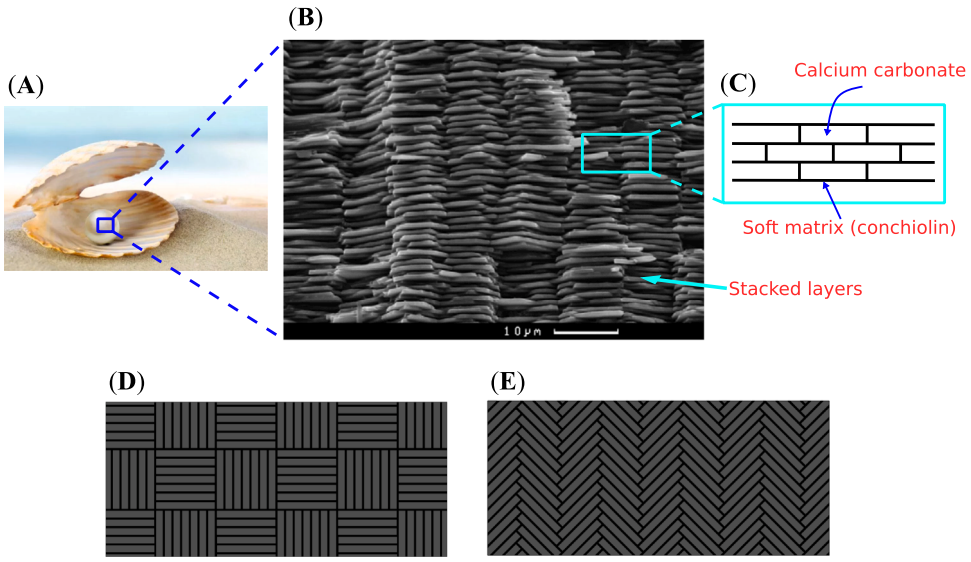

Fig. 1. Design inspiration from natural nacre and the proposed composite architectures. (B) SEM image of natural nacre showing its hierarchical brick-and-mortar structure composed of aragonite platelets and soft organic layers (adapted from [43]). (C) Schematic of the nacre architecture, where platelet sliding enables energy dissipation and toughening. (D, E) Proposed designs studied in this work, including the crosshatch, and herringbone geometries, all fabricated via additive manufacturing and evaluated under uniaxial tension to compare their fracture behavior.

could have accomplished as good performance as nacre with such a high hard material composition [20,44,45]. Nacre's non-brittle behavior can be attributed to the biological soft protein binding constituent comprising approximately 5% of its volume. It works as a glue agent (approximately 20 nm in thickness) between mineral inclusions, making the structure more damage-tolerant and distributing loads among brittle platelets, where Tushtev et al. [43] found that the biopolymer matrix plays a major role in the stress distribution. Barthelat [46] postulated a multi-objective optimization guidelines embracing inclusions and matrix materials properties as design parameters. One of these guidelines revealed that the staggered microstructure is effective only when the inclusions are at least five times stronger than the interfaces.

Due to its intricate hierarchical structure and unique characteristics, nacre has earned significant interest from biology scientists, materials researchers, and engineers [40]. Mayer [47] studied the mechanisms underlying the toughness of nacre. They suggested that crack diversion and energy dissipating processes take leading roles in improving toughness of these composites. Further, [47] underlined that its hierarchical design and soft protein matrix increase its energy dissipation. [48] investigated the impact resistance of nacre-like architectures across a range of impact velocities. They observed that while these structures effectively dissipate energy through tablet sliding at low impact velocities, their resistance decreases beyond a critical threshold. At higher impact velocities, deformation becomes more localized, reducing the overall energy dissipation capability compared to traditional laminated structures. [49] investigated a nacre-inspired composite for blast-resistant applications, demonstrating enhanced energy dissipation and improved structural performance under impulsive loading. Numerical analysis revealed that the hierarchical design increases resistance to failure while reducing deformation, attributed to interlayer interactions and toughening mechanisms.

Abid et al. [50] studied the influence of microstructure randomness on the fracture of nacre-like composites via discrete element modeling. They found slight randomness in the microstructure increases toughness. However, higher microstructure randomness creates very weak zones, leading to a reduction in toughness. Their findings imply that the microstructure's randomness should be kept to a minimum to acquire the best performance. Poloni et al. [51] fabricated nacre-like composites using alumina platelets glued by iron as the cementing agent. Their composites showed exceptional fracture resistance, yet have lightweight, with thermal and magnetic properties.

A micromechanical analysis was conducted by Slesarenko et al. [52] to investigate the performance of nacre-like composites. Their inclusions are created from hard fillers, while the soft interface is made from vulcanized natural rubber. Their study was composed of two parts: computational and experimental. The computational part was conducted employing continuum mechanics and adopting energy limiters [53–55] together with high-fidelity generalized method of cells. Alternatively, the experimental part was conducted on 3D-printed composites to validate their numerical findings. They concluded that the composite overall strength is determined by shear and tensile deformation of the soft interface. In [56], they conducted finite element and experimental studies and concluded that nacre-like composites demonstrate high toughness when the inclusions have small inclination angles.

The shear-lag model has long been employed to understand the load transfer mechanisms in composite materials, offering key insights into their mechanical properties [57–65]. Kotha et al. [66] developed a micromechanical model using shear-lag theory to study load transfer in composites reinforced with rectangular platelets. Their research examined how factors such as matrix stiffness and reinforcement volume fraction influence the distribution of shear and axial stresses. They also investigated how platelet aspect ratio, volume fraction, and overlap affect the overall elastic modulus of the composite. While their model's predictions for axial load transfer closely matched results from finite element analysis (FEA), discrepancies in interfacial shear stress transfer appeared at lower volume fractions. This model was further applied to study the mechanical behavior of bone tissue at the ultrastructural level, simulating interactions between mineral platelets within an organic matrix [66]. The shear-lag model has also been used to study nacre and nacre-inspired composites [67–72]. For example, Jackson et al. [39] tested nacre-like models made from glass slides and compared the experimental results with theoretical predictions for platelet-reinforced composites. Their findings confirmed that the shear-lag model accurately predicted the Young's modulus, and tensile failure was explained by a shear transfer mechanism. Despite challenges in replicating nacre's fracture toughness due to scaling issues, the study suggested that delamination in materials with low span-to-depth ratios could enhance toughness. Similarly, Ji and Gao [68] applied a tension-shear chain (TSC) model to understand the behavior of protein-mineral nanocomposites. Their research highlighted the importance

of optimizing the tensile strength of nanoscale mineral crystals to improve material strength, with smaller crystals less prone to flaws, thereby approaching the theoretical strength of atomic bonds. This modification improved fracture toughness by enabling energy dissipation through shear deformation in the protein matrix. They also derived the viscoelastic properties of the composite, showing that the viscoelasticity of the protein further contributes to enhanced toughness. Recently, shear-lag models have been extensively employed to model the mechanical behavior of nacre-inspired composites [73–85]. These models provide valuable insights into how stress is distributed between the stiff platelets and the soft matrix, helping to explain the enhanced toughness observed in such bioinspired materials.

Fracture evolution simulations were conducted by Abu-Qbeitah et al. [16] in nacre-like composites as well as in proposed designs using the material-sink approach [12–15]. They concluded that the nature-choice design in nacre is the best one among the examined designs. It is the best in terms of the maximum bearing stress, the highest energy dissipating due to fracture, encompasses multiple steps of fracture — rather than one-step catastrophic fracture, and giving warning signs before the full separation of the sample.

Different microstructures (flat, dovetail, inverse-dovetail) have been numerically analyzed by [86]. The study concluded that the inverse-dovetail design demonstrates outstanding impact stiffness, whereas the dovetail design shows higher energy absorption. In each case of the latter study, the inclusion design is changed. However, it would be interesting to study the effect of the design itself while keeping the same inclusion design in all cases. Furthermore, the latter study was conducted via finite element simulations, where physical experiments will represent the real behavior. Thus, in the current study, different microstructures will be experimentally tested, while keeping the inclusions design the same in all cases as shown in Fig. 1.

Additive manufacturing (i.e., 3D printing) has recently been employed to fabricate platelet-stiffened soft composites due to their reasonable cost and lower carbon footprint compared to conventional manufacturing methods [87–94]. It can reduce manufacturing costs by up to 40% [95]. Initially, this technology was used for producing polymer prototypes and has since progressed to include thermoplastics, metals, and ceramics [96].

The present work employs multimaterial 3D printing to fabricate soft composites inspired by natural designs. The first objective is to experimentally assess the performance of a nacre-like design in comparison to newly proposed geometries. The second objective is to validate the numerical predictions presented in [16], which employed the novel Material Sink (MS) fracture modeling approach implemented in the commercial finite element software Abaqus. The third objective is to experimentally investigate the rate-dependent response of nacre-like composites under uniaxial tensile loading.

To this end, we fabricate a series of bioinspired composites consisting of rigid inclusions embedded in a soft matrix, mimicking the brick-and-mortar structure of natural nacre. These structures are subjected to tensile tests until complete fracture, and their mechanical performance – stiffness, strength, stretchability, and fracture toughness – is quantified and compared. The experimental results are interpreted using the MS fracture modeling framework, and the influence of loading rate is examined over a wide dynamic range. Notably, we report the first experimental observation of inclusion fracture at high strain rates, revealing a critical limitation of this otherwise robust design.

The structure of the paper is organized as follows. Section 2 describes the materials, experimental setup, and methodology employed in this study. Section 2.1 presents the mechanical testing results for various composite designs and compares them with the numerical predictions from [16]. Section 2.2 investigates the strain-rate-dependent fracture behavior of the nacre-like composite and its constituent materials. A detailed discussion of the underlying mechanisms and broader implications is provided in Section 3, followed by the main conclusions in Section 4.

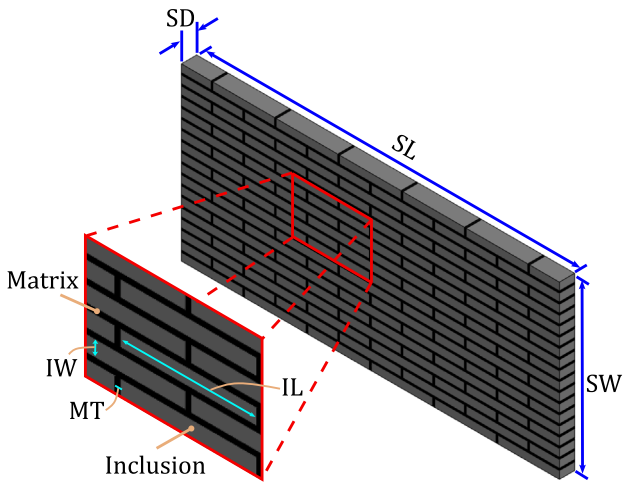

Fig. 2. Geometry of the 3D-printed composite with a nacre-like architecture. Gray regions represent rigid VeroUltraWhite inclusions arranged in a staggered pattern, while black regions indicate the soft ElasticoClear matrix. This design mimics the hierarchical structure of natural nacre and is used to study fracture behavior under uniaxial loading.

2. Experiments

This section describes the fabrication and testing procedures used to evaluate the mechanical performance of nacre-inspired composites. The workflow includes model design, multimaterial 3D printing, post-processing (curation), and uniaxial tensile testing. The materials used for the soft matrix and rigid inclusions are specified, and typical print and cure times are reported.

A Stratasys J35 Pro 3D printer is used to fabricate composite samples for mechanical testing. The 3D models are designed using SolidWorks and imported into the printer via GrabCAD Print software. The printer uses cartridges of structural and support materials,[1] as well as a waste container. Notably, the printer allows for the creation of custom material properties by blending structural materials in defined ratios.

The matrix and inclusions are fabricated from ElasticoClear (FLX934) and VeroUltraWhite (RGD824), respectively. According to the manufacturer's data sheets [97], ElasticoClear has a tensile strength of 4 ± 1 MPa and a stretch at fracture of 3.8 ± 0.2, while VeroUltraWhite has a tensile strength of 57.5 ± 7.5 MPa and a stretch at fracture of 1.125 ± 0.075. The soluble support material SUP710 is used and easily removed after printing.

The curation process is design-specific, while the printing time depends on sample size and the number of layers. On average, each sample requires approximately 2 h to print and 12 h for curing. Following curation, the samples are tested within 24 h.

2.1. Fracture toughening mechanisms of nacre-like design versus other alternative designs

A considerable amount of energy has been proven to be dissipated by nacre-like structures through inclusions sliding [98], however, whether other architectures will demonstrate comparable behavior remains unclear. In this subsection, new designs, other than the nacre (offset) design are tested until full fracture. Their strengths, fracture toughness, and crack paths are investigated experimentally. Two designs, modeled by [16], are fabricated and tested in uniaxial tension.

[1] Material that is either built under overhanging features or as infill to support structural materials.

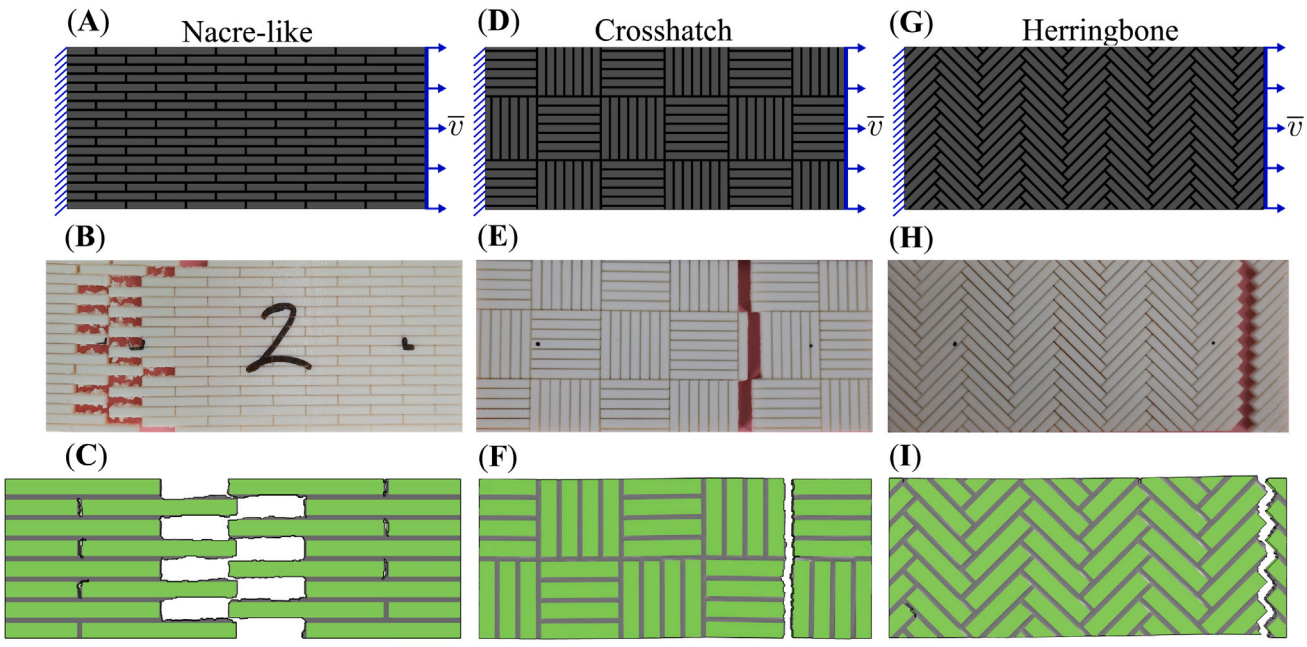

Fig. 3. Geometric configurations for the (A) nacre-like (offset), (D) crosshatch, and (G) herringbone designs. Gray indicates rigid inclusions, while black represents the soft matrix. Experimentally observed fracture paths are shown for the (B) nacre-like, (E) crosshatch, and (H) herringbone samples. Corresponding fracture paths from numerical simulations using the Material-Sink (MS) modeling framework [16] are presented in (C), (F), and (I) (reprinted with permission).

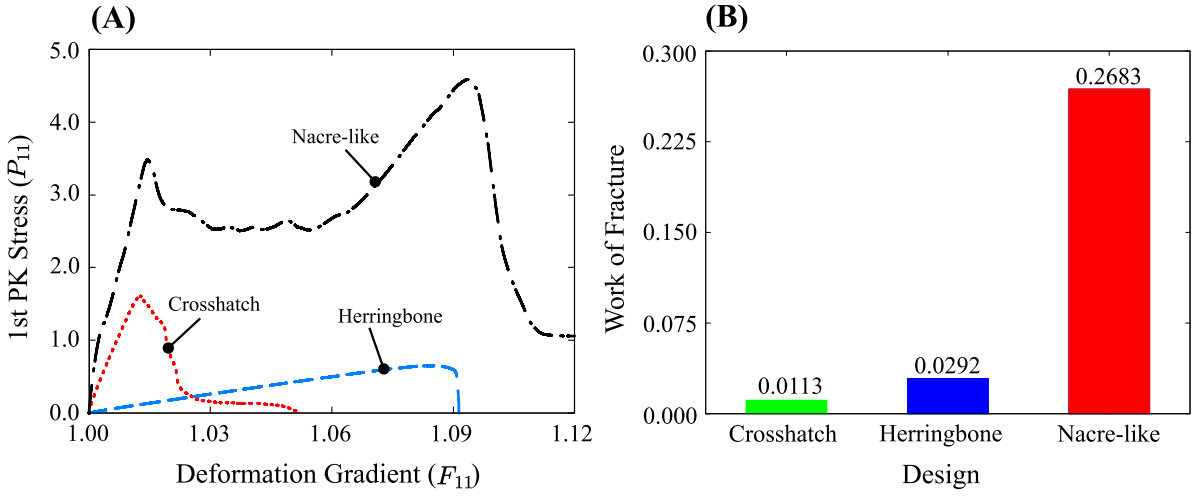

Fig. 4. Mechanical performance of three composite designs under uniaxial tension. (A) First Piola–Kirchhoff stress (MPa) plotted against the deformation gradient in the loading direction for nacre-like, crosshatch, and herringbone geometries, showing their distinct stress–strain responses. (B) Corresponding volumetric work of fracture (mJ/mm^3), quantifying energy absorption per unit volume. Data highlight the superior toughness of the nacre-like design compared to alternatives.

The first design is the offset deign, where the geometric setup of the sample is depicted in Fig. 2, illustrating the offset design observed in natural nacre. The specimen has an offset (mortar-block) structure with a soft matrix stiffened by hard inclusions, arranged as shown in Fig. 2, where the matrix and inclusions are designated with black and gray colors, respectively. The sample length (SL), sample width (SW), and sample depth (SD) are 98.5 mm, 44.5 mm, and 4 mm, respectively. The inclusion length (IL), inclusion width (IW), and matrix thickness (MT) are 16 mm, 2 mm, and 0.5 mm, respectively, where these dimensions were adopted from [56].

The sample is tested in uniaxial tension using the Instron 34SC-5 universal testing machine. A strain rate $\dot{\varepsilon} = 10^{-5}$ s^{-1} is applied on the right edge, along the sample's length direction, while the left edge is fixed. The strain rate was chosen to be low enough to diminish any rate-dependent behavior of the matrix and filler materials [99,100]. Fig. 4 shows the 1st Piola–Kirchhoff stress component (P_{11}) versus deformation gradient component (F_{11}) curve. It can be noted that damage occurs on two steps. The first step is by fracturing the short edges of the matrix that are perpendicular to the tensile loading. Subsequently, the short edges connect along the matrix's long edges until full separation, as shown in Fig. 3 (B). In this nacre-like design, most of the sample resists fracture by breaking all the short edges first before localizing the crack to a specific part of the sample.

The second design is crosshatch pattern, as shown in Fig. 3(D). The sample dimensions, inclusion dimensions, and matrix width are the same as those of the offset pattern shown in Fig. 2. The sample is under a uniaxial tension in the horizontal direction applying on the right edge with a strain rate $\dot{\varepsilon} = 10^{-5}$ s^{-1}, while the left edge is fixed. The crack initiates within the soft matrix in a fairly straight path, which is perpendicular to the tensile loading until the full separation, as shown

in Fig. 3(E). The 1st Piola–Kirchhoff stress component (P_{11}) versus deformation gradient component (F_{11}) curve is shown in Fig. 4, where the stress keeps increasing until reaching a maximum point, followed by a stress drop. It can be observed that the damage occurs in a single catastrophic fracture, rather than in multiple steps as previously seen in the nacre-like pattern.

The geometric setup of the herringbone design is shown in Fig. 3(G), where a strain rate of $\dot{\varepsilon} = 10^{-5}$ s^{-1} is applied on the right edge, while the left edge is fixed. The inclusions are inclined at 45°with dimensions as adopted for the nacre-like pattern shown in Fig. 2. The crack initiates within the matrix and propagates in a zigzag pattern following the twining of the matrix, as shown in Fig. 3(H). The 1st Piola–Kirchhoff stress component (P_{11}) versus deformation gradient component (F_{11}) curve is shown in Fig. 4(A), where it exhibits a one-step fracture.

It can be noted that the crosshatch design demonstrates stiffness more comparable to the nacre-like pattern. The latter is attributed to the absence of shearing in the long interfaces in the crosshatch pattern. However, the strain at which the sample fractures is almost one-third of what is achieved by the nacre-like design. It is evident that the nacre-like design not only results in a higher stiffness response compared to other designs but also leads to greater deformation at fracture, as shown in Fig. 4(A).

Remark. In this study, we use the deformation gradient to characterize the deformation rather than principal stretches or strain measures. While strain-based approaches are more commonly used, the deformation gradient is specifically chosen because it is work-conjugate with the First Piola–Kirchhoff stress. This selection ensures a consistent and rigorous formulation within our framework, particularly when analyzing the mechanical response under finite deformations. By maintaining this conjugacy, we provide a more physically meaningful representation of the stress–deformation relationship in our system.

Figs. 3(C), (F), and (I) depict the damage patterns for the nacre-like, crosshatch, and herringbone designs, respectively, as predicted by the Material-Sink (MS) modeling framework [16]. The fracture paths observed in our experiments closely align with those predicted by the simulations, thereby validating the accuracy of the MS approach in fracture modeling.

Fig. 4(B) illustrates the volumetric work of fracture, determined by integrating the areas under the stress–strain curves for each design up to their respective failure points. The crosshatch design exhibits a work of fracture of 0.0113 mJ/mm^3, which is less than 40% of the value observed for the herringbone design. Remarkably, the nacre-like design demonstrates a significantly higher work of fracture than both the crosshatch and herringbone designs, as shown in Fig. 4(B). This suggests that the nacre-like design offers superior stiffness, strength, and toughness relative to the other proposed geometries.

2.2. Time-dependent fracture behavior of nacre-like structures

As previously mentioned, the nacre-like design consists of hard fillers embedded in a soft matrix, as illustrated in Fig. 3(A). Prior to investigating the time-dependent behavior of the nacre-like design, the uniaxial viscoelastic responses of the composite constituents are examined individually.

Figs. 5(A) and (B) show the 1st Piola–Kirchhoff stress component (P_{11}) versus deformation gradient component (F_{11}) curves in uniaxial tension of both the hard material (VeroUltraWhites) and the soft material (ElasticoClear), respectively, at various strain rates. For the VeroUltraWhites, increasing the strain rate increases the material's stiffness and fracture stress (Fig. 5(E)), yet the total strain at which the material is fully fractured decreases (Fig. 5(C)). It is also noted that the samples at low strain rates demonstrate large plastic dissipation zone. It can also be concluded that VeroUltraWhites material exhibits a time-dependent response.

For ElasticoClear, increasing the strain rate leads to higher fracture stress (Fig. 5(F)) and fracture strain (Fig. 5(D)), while the stiffness remains nearly unchanged across all cases. This behavior contrasts with the well-established response of standard viscoelastic soft materials, where failure strain typically decreases at higher strain rates due to reduced molecular relaxation time. Interestingly, the material appears to sustain increasing levels of strain as strain rate rises, theoretically trending toward infinity. A similar trend was reported by Slesarenko and Rudykh [101] for TangoPlus material, suggesting that this may be an intrinsic characteristic of digital 3D-printed soft materials.

At the material level, this unconventional rate dependence suggests that ElasticoClear exhibits a unique viscoelastic response under dynamic loading. The polymer network structure, crosslink density, and molecular relaxation mechanisms may all contribute to this effect. Unlike many soft materials that exhibit strain localization and premature failure at high strain rates, ElasticoClear appears to dissipate energy more effectively, delaying fracture and allowing for larger deformations before failure. However, due to the limited availability of high-strain-rate data for ElasticoClear in the literature, direct comparisons remain challenging. Notably, while Slesarenko and Rudykh (2018) observed a similar effect, the phenomenon appears significantly more pronounced in our case.

At the experimental level, factors such as strain-rate-dependent viscoelastic stiffening may also play a role. Additionally, at higher strain rates, the material may exhibit enhanced viscoelastic stiffening, which could contribute to the observed increase in both stress and strain at fracture. To further understand the origins of this behavior, future studies should focus on comprehensive viscoelastic characterization across a broader range of strain rates, as well as numerical modeling to isolate material-specific effects from experimental influences. Nevertheless, our results demonstrate that ElasticoClear exhibits a distinct and complex rate-dependent response, warranting further investigation into its high-strain-rate mechanical properties.

After analyzing the time-dependent responses of the individual constituents, the time-dependent behavior of the nacre-like composites is investigated. The geometric configuration of all samples is shown in Fig. 2. Tensile strain rates of 10^{-4}, 10^{-3}, and 10^{-2} s^{-1} are applied to the right edge in the direction parallel to the sample's length (SL), while the left edge is fixed, preventing movement in the x, y, and z directions.

Fig. 6(A) shows 1st Piola–Kirchhoff stress component (P_{11}) vs deformation gradient component (F_{11}) curves for different values of applied strain rates. The first notice is that in all cases, the two peaks exist on the stress–deformation gradient curves, whether the strain rate is small or high. The initial peak marks the onset of damage at the matrix's short edges, leading to a decline in stress until it reaches a minimum. Following this, shear deformation along the composite's long edges becomes the primary mechanism, causing stress to rise until the second peak is reached. At this point, the material reaches its maximum strength, resulting in complete failure. It can be noticed that applying higher strain rates shifts the graphs upward due to the over-stress contribution induced by the viscosity. Figs. 6(B), (C), and (D) show fracture paths for applied strain rates of 10^{-4}, 10^{-3}, 10^{-2} s^{-1}, respectively. It is noticed that increasing the strain rate urges localizing damage within the inclusions rather than the matrix, where such fracture encompasses considerable debris.

To investigate the influence of curing conditions on the mechanical response, we tested a second group of samples produced under different conditions. Case II was tested where the curation time was doubled, and its response is shown in Fig. 6(E). The same observation was made: at high strain rates, the samples tolerate higher stresses without a corresponding decrease in strain. The resulting fracture paths, shown in Figs. 6(F-H), confirm the same observation of inclusion fracture at high strain rates. This represents the first observation of fracture occurring within the inclusions rather than the matrix in nacre-like composites. The variation in failure behavior observed in Figs. 6(C) and (G), despite

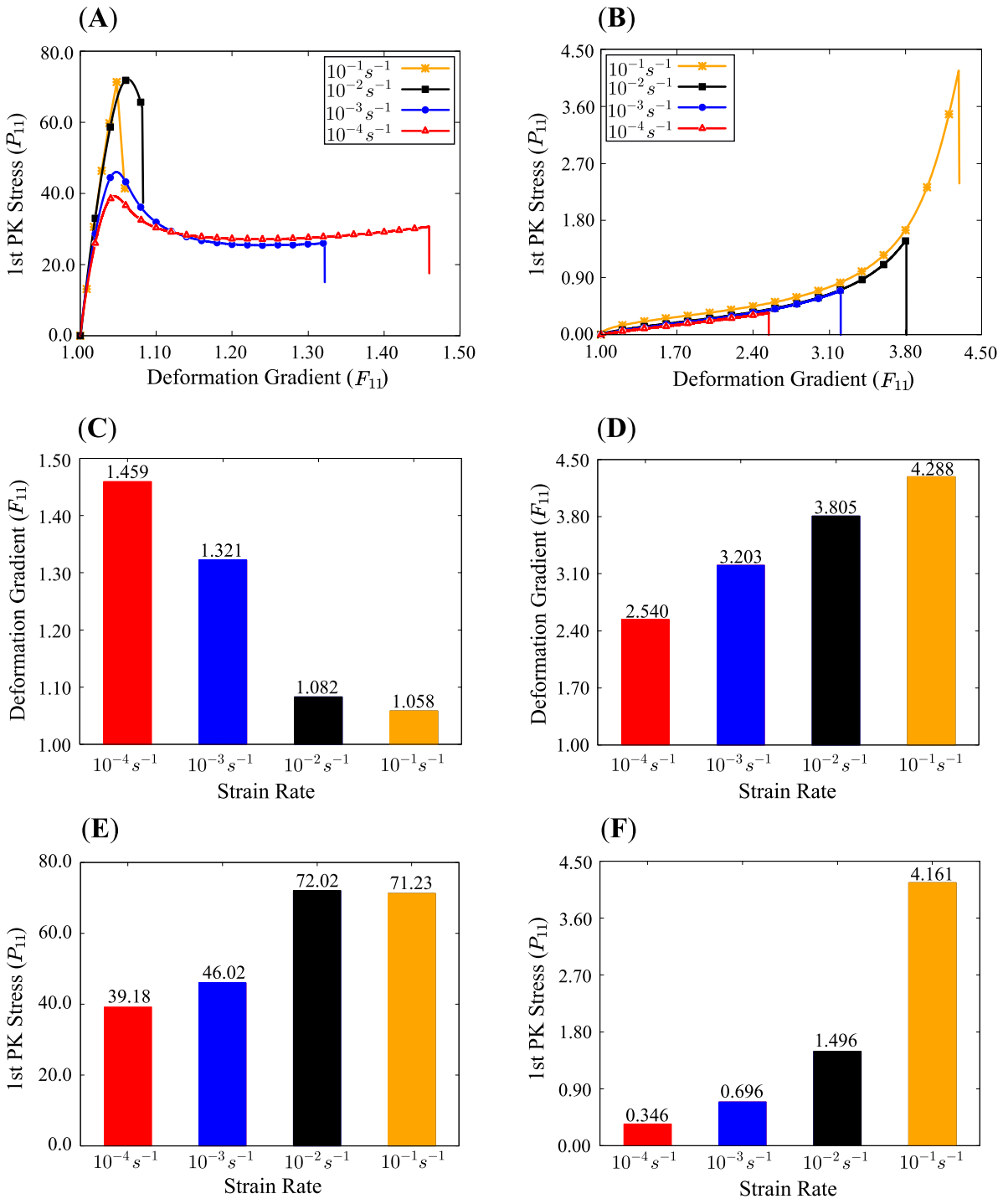

Fig. 5. 1st Piola–Kirchhoff stress component (MPa) versus deformation gradient component in the loading direction during uniaxial tension tests for (A) VeroUltraWhite (RGD824) and (B) ElasticoClear (FLX934) at various strain rates. Panels (C) and (D) show the maximum deformation achieved under different strain rates for VeroUltraWhite and ElasticoClear, respectively. Panels (E) and (F) present the corresponding maximum stress values across the strain rates for the two materials.

identical strain rates, stems from a critical phenomenon. At intermediate strain rates, a "boundary" case emerges, where the competition between stress redistribution and fracture dynamics allows cracks to propagate through any phase. This transitional behavior underscores the complex interplay of material properties and loading conditions in determining fracture pathways.

Tables 2 and 3 present the measured static toughness (distinct from the intrinsic fracture toughness of the material) and tensile strength for both cases. The data clearly indicate an increasing trend in both properties as the strain rate rises. This suggests that the material exhibits strain-rate-dependent toughening and strengthening mechanisms, likely influenced by the dynamic interaction between the brick-and-mortar architecture and the soft interface.

It is important to note that in all the previous cases, fracture initiated by damaging the short edges of the matrix, even at high strain rates. The fracture then progressed either by damaging the long edges

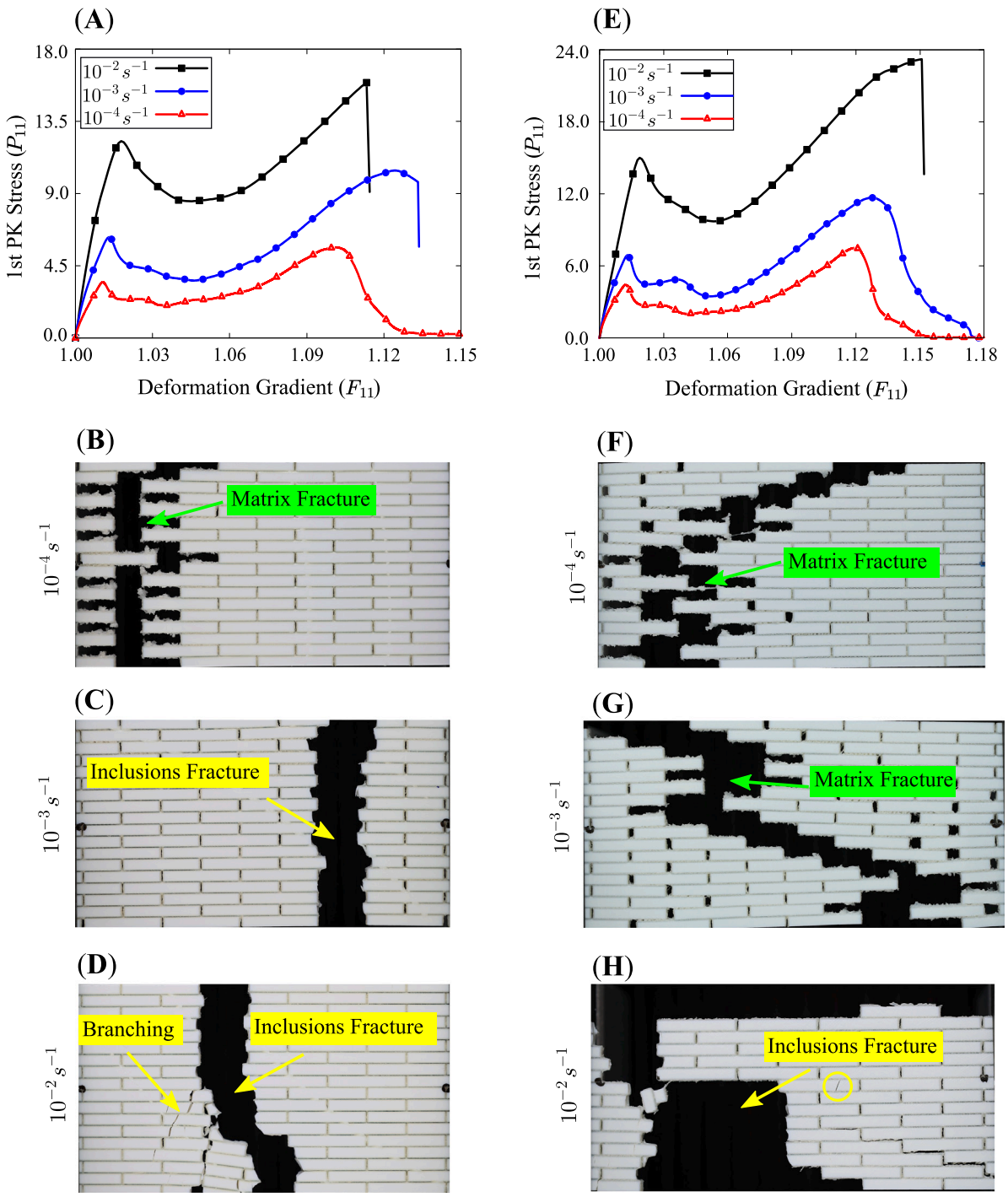

Fig. 6. Time-dependent mechanical responses for the first case: (A) 1st Piola–Kirchhoff stress component (MPa) versus deformation gradient component in the loading direction; (B), (C), and (D) show fracture paths corresponding to applied strain rates of 10^{-4}, 10^{-3}, and 10^{-2} s^{-1}, respectively. Time-dependent responses for the second case: (E) 1st Piola–Kirchhoff stress component (MPa) versus deformation gradient component; (F), (G), and (H) display fracture paths for the same strain rates as above. The results highlight strain-rate-dependent fracture behavior, with cracks propagating primarily through the soft matrix at low strain rates and shifting to the hard inclusions at higher strain rates, indicating a transition from ductile to brittle failure modes.

of the matrix, leaving the inclusions intact (matrix fracture at low strain rates), or by cutting through the platelets (inclusion fracture at high strain rates).

The observed dynamic failure mechanisms in nacre-like composites have significant implications for mechanical engineering applications that demand high impact resistance and efficient energy dissipation. The ability of these structures to shift between failure modes – matrix-dominated at low strain rates and inclusion-dominated at higher strain rates – demonstrates their adaptability to varying loading conditions. This makes them highly relevant for applications in aerospace and automotive engineering, where materials must withstand impact forces, absorb energy effectively, and prevent catastrophic failure. Additionally, the study underscores the critical role of interfacial properties in governing fracture behavior, offering valuable insights for the design of advanced bioinspired composites with superior toughness, durability, and performance under dynamic loading conditions.

Table 1
Fracture type in nacre-like composite tested for different strain rates in uniaxial tension.

	10^{-4} s^{-1}	10^{-3} s^{-1}	10^{-2} s^{-1}
Case I	Matrix	Inclusion	Inclusion
Case II	Matrix	Matrix	Inclusion

Table 2
Static toughness (measured in mJ/mm^3) for both cases of nacre-like composites.

	10^{-4} s^{-1}	10^{-3} s^{-1}	10^{-2} s^{-1}
Case I	0.312	0.718	1.157
Case II	0.417	0.785	2.148

Table 3
Strength (measured in MPa) for nacre-like composites.

	10^{-4} s^{-1}	10^{-3} s^{-1}	10^{-2} s^{-1}
Case I	5.653	10.439	15.907
Case II	7.490	11.697	23.201

3. Discussion

3.1. Viscoelastic behavior under dynamic loading

The mechanical response of nacre-like structures under dynamic loading is significantly influenced by viscoelastic effects, particularly due to the time-dependent behavior of the soft interface and hard inclusions materials. Viscoelastic materials exhibit both elastic and viscous characteristics, leading to strain-rate-dependent mechanical properties that influence fracture mechanisms and energy dissipation.

At low strain rates, the material has sufficient time to relax, allowing for greater interfacial sliding and energy dissipation through frictional mechanisms. However, at higher strain rates, the viscoelastic nature leads to a stiffer response, reducing energy dissipation through sliding while promoting localized stress concentrations in inclusions.

Experimental observations in this study confirm these theoretical expectations. The transition from matrix-dominated failure at low strain rates to inclusion-driven crack localization at higher strain rates can be attributed to the viscoelastic stiffening, which alters stress redistribution and fracture propagation dynamics. The increased stiffness at high strain rates reduces the effectiveness of energy dissipation mechanisms that typically enhance toughness in bioinspired composites.

To further quantify these effects, future studies could incorporate time-dependent material characterization (e.g., dynamic mechanical analysis) and numerical simulations incorporating viscoelastic constitutive models. Such an approach would provide deeper insights into the role of viscoelasticity in governing the dynamic failure mechanisms of nacre-like materials, enabling better predictive modeling for high-performance impact-resistant applications.

3.2. Microscopic mechanisms underlying macroscopic behavior

The macroscopic behavior observed in nacre-inspired composites – particularly their enhanced toughness, progressive failure, and rate-dependent fracture patterns – can be directly attributed to microscopic interactions between the hard inclusions and soft matrix. These interactions are governed by the architecture of the composite, the contrasting mechanical properties of the constituent materials, and their response to different loading rates.

At the microscale, the nacre-like architecture promotes a sequential failure process that distributes damage over a larger volume. Under tension, the short edges of the soft matrix first yield and initiate local damage. This early-stage failure is not catastrophic but instead triggers a redistribution of stresses along the longer interfaces. Microscopically, this promotes shear deformation in the soft phase and stress transfer into the inclusions, which are more capable of bearing load. This progressive engagement of the microstructure delays catastrophic failure and increases the overall energy absorption capacity, as evidenced by the two-peak stress response observed in the experiments.

In contrast, alternative designs lacking this layered geometry fail abruptly, with fracture confined to a narrow damage zone. This indicates that without a well-organized microstructural mechanism for stress redistribution – such as the angled brick arrangement in nacre – the material cannot utilize its full energy dissipation potential. The absence of staged failure mechanisms at the microscale leads to sudden macroscopic failure.

Strain rate further modulates the microscopic failure mechanisms. At low strain rates, the soft matrix has sufficient time to deform plastically and absorb energy, causing failure to propagate primarily through the matrix. However, as strain rate increases, the matrix stiffens while the inclusions begin to dominate the load-bearing response. This shift leads to fracture localization within the inclusions – despite their higher strength – due to their more brittle behavior and reduced ability to dissipate energy dynamically. At intermediate strain rates, both phases are active participants in the failure process, resulting in a mixed fracture mode. This transition highlights the importance of time-dependent material behavior at the microscale and its impact on the global mechanical response.

Altogether, the experimental findings reveal that the macroscopic toughness and failure evolution of the nacre-like composite are intimately connected to how its microscopic architecture mediates stress distribution, deformation localization, and energy dissipation. By tuning the microstructure and understanding the relative contributions of matrix and inclusions under dynamic conditions, the design of architected materials can be optimized for application-specific loading regimes.

4. Conclusions

This study set out to explore how architectural design and strain rate influence the mechanical behavior of soft interface composites inspired by natural nacre. Specifically, we aimed to identify whether alternative designs could match the toughening mechanisms of nacre-like structures and how strain rate impacts fracture paths across different phases.

3D-printed soft interface composites were tested under uniaxial tension to evaluate their mechanical properties. Nacre-like structures, along with alternative proposed designs, were analyzed to assess their tensile strength, deformation behavior, and failure modes.

The results revealed that the nacre-like design undergoes fracture in two distinct steps. Initially, the short edges of the matrix fail, followed by fracture localization and propagation parallel to the applied load. The initial peak marks the onset of damage at the matrix's short edges, leading to a decline in stress until it reaches a minimum. Following this, shear deformation along the composite's long edges becomes the primary mechanism, causing stress to rise until the second peak is reached. At this point, the material reaches its maximum strength, resulting in complete failure. This failure sequence engages the majority of the sample in resisting the damage, effectively enhancing fracture toughness and validating the results from MS modeling. These observations directly support our hypothesis that nacre-inspired architectures can delay and distribute failure through progressive engagement of toughening mechanisms.

The proposed designs experienced sudden, catastrophic failure, characterized by an abrupt breakdown without prior warning. Damage was confined to a localized region of the sample, in contrast to the more distributed failure observed in the nacre-like composites. In comparison, the nacre-like design demonstrated superior performance, exhibiting higher strength and stiffness. This design underwent fracture in multiple stages, providing warning signs before complete failure and ultimately enhancing the overall toughness of the sample. Notably, the

work of fracture for the nacre-like design was almost ten times greater than that of any other tested configuration. This confirms our initial aim to benchmark the toughness of alternative geometries against the nacre pattern, showing that architectural biomimicry remains unmatched in performance.

The rate-dependent behavior of the nacre-like composites was investigated, revealing that fracture initiation occurs through localization at the short edges. At lower strain rates, failure propagates through the matrix, whereas at higher strain rates, fracture predominantly occurs within the inclusions, as summarized in Table 1. It is important to note that at intermediate strain rates, a 'boundary' case arises, allowing cracks to propagate through any phase. To the best of the authors' knowledge, this behavior has not been previously documented in the literature. This phenomenon is likely attributed to the differential response of the soft matrix and the rigid inclusions to the increasing strain rate, highlighting the contrasting mechanical properties of the phases involved. These findings align with our hypothesis that strain rate would influence the active fracture phase and provide new insights into transition behaviors at intermediate rates.

Overall, this work demonstrates that nacre-like geometries not only provide superior toughness but also introduce rate-dependent fracture pathways that may be exploited in future designs. These results support the development of architected composites tailored for load-bearing applications under varying dynamic conditions.

CRediT authorship contribution statement

Suhib Abu-Qbeitah: Writing – review & editing, Writing – original draft, Visualization, Validation, Methodology, Investigation, Formal analysis, Conceptualization. **Olga Petrenko:** Investigation, Formal analysis, Validation. **Konstantin Y. Volokh:** Writing – review & editing, Methodology, Conceptualization. **Stephan Rudykh:** Writing – review & editing, Project administration, Methodology, Conceptualization, Funding acquisition.

Declaration of competing interest

The authors declare that they have no known competing financial interests or personal relationships that could have appeared to influence the work reported in this paper.

Acknowledgments

The support from the European Research Council (ERC) under the European Union's Horizon 2020 research and innovation programme (MAGIC –[852281]) is gratefully acknowledged. Also, K. Y. Volokh is supported by the Israel Science Foundation, Israel (ISF-394/20) as well as the Israeli Ministry of Science and Technology, Israel (MOST-0005173).

Data availability

Data will be made available on request.

References

[1] Ashby MF, Cebon D. Materials selection in mechanical design. J Phys IV Fr 1993;03(C7):C7–1–C7–9. http://dx.doi.org/10.1051/jp4:1993701.

[2] Wiener J, Arbeiter F, Pinter G. Concepts towards bio-inspired multilayered polymer-composites. Procedia Struct Integr 2023;47:253–60. http://dx.doi.org/10.1016/j.prostr.2023.07.018, 27th International Conference on Fracture and Structural Integrity (IGF27).

[3] Niu X, Xu F, Zou Z, Zhu Y, Duan L, Du Z, Ma H. Mechanical properties of horsetail bio-inspired honeycombs under quasi-static axial load. Int J Mech Sci 2023;260:108663. http://dx.doi.org/10.1016/j.ijmecsci.2023.108663.

[4] Isaac CW, Duddeck F, Ha NS. Axial crushing response of novel toothed gear bio-inspired 3D printed energy absorbing structures. Int J Mech Sci 2025;288:110033. http://dx.doi.org/10.1016/j.ijmecsci.2025.110033.

[5] Wang P, Yang F, Li P, Zhang W, Lu G, Fan H. Bio-inspired vertex modified lattice with enhanced mechanical properties. Int J Mech Sci 2023;244:108081. http://dx.doi.org/10.1016/j.ijmecsci.2022.108081.

[6] Shteinberg G, Haj-Ali R, Libonati F, Sharabi M. Plant biomimetic principles of multifunctional soft composite development: A synergistic approach enabling shape morphing and mechanical robustness. ACS Biomater Sci Eng 2024;10(6):3707–17. http://dx.doi.org/10.1021/acsbiomaterials.3c01163.

[7] Rudykh S, Ortiz C, Boyce MC. Flexibility and protection by design: imbricated hybrid microstructures of bio-inspired armor. Soft Matter 2015;11:2547–54. http://dx.doi.org/10.1039/C4SM02907K.

[8] Liu G, Ghosh R, Vaziri A, Hossieni A, Mousanezhad D, Nayeb-Hashemi H. Biomimetic composites inspired by venous leaf. J Compos Mater 2018;52(3):361–72. http://dx.doi.org/10.1177/0021998317707254.

[9] Ali H, Ebrahimi H, Ghosh R. Bending of biomimetic scale covered beams under discrete non-periodic engagement. Int J Solids Struct 2019;166:22–31. http://dx.doi.org/10.1016/j.ijsolstr.2019.01.021.

[10] Wertheimer S, Sharabi M, Shelah O, Lesman A, Haj-Ali R. Bio-composites reinforced with unique coral collagen fibers: Towards biomimetic-based small diameter vascular grafts. J Mech Behav Biomed Mater 2021;119:104526. http://dx.doi.org/10.1016/j.jmbbm.2021.104526.

[11] Zhang X, Han Y, Zhu M, Chu Y, Li W, Zhang Y, et al. Bio-inspired 4D printed intelligent lattice metamaterials with tunable mechanical property. Int J Mech Sci 2024;272:109198. http://dx.doi.org/10.1016/j.ijmecsci.2024.109198.

[12] Volokh KY. Fracture as a material sink. Mater Theory 2017;1(1):3. http://dx.doi.org/10.1186/s41313-017-0002-4.

[13] Abu-Qbeitah S, Jabareen M, Volokh KY. Quasi-static crack propagation in soft materials using the material-sink theory. Int J Mech Sci 2023;248:108160. http://dx.doi.org/10.1016/j.ijmecsci.2023.108160.

[14] Abu-Qbeitah S, Jabareen M, Volokh KY. Dynamic versus quasi-static analysis of crack propagation in soft materials. J Appl Mech 2022;89(12):121008.

[15] Abu-Qbeitah S, Jabareen M, Volokh KY. Modeling cracks in viscoelastic materials at finite strains. Internat J Numer Methods Engrg 2024;125(5):e7398. http://dx.doi.org/10.1002/nme.7398.

[16] Abu-Qbeitah S, Jabareen M, Volokh KY. On strength and toughness of soft staggered composites. Mech Mater 2024;191:104935. http://dx.doi.org/10.1016/j.mechmat.2024.104935.

[17] Wang C, Zheng D, Zhang C, Gu L, Shu K, Aldakheel F, Wriggers P. A general phase-field model for simulating impact-sliding contact failure. Int J Mech Sci 2024;273:109215. http://dx.doi.org/10.1016/j.ijmecsci.2024.109215.

[18] Abu-Qbeitah S, Volokh KY, Rudykh S. Energy-based versus stress-based material failure criteria: the experimental assessment. Mech Res Commun 2025;148:104445. http://dx.doi.org/10.1016/j.mechrescom.2025.104445.

[19] Pure Pearls. Pearl nacre: The building blocks of beauty URL https://www.purepearls.com/pages/pearl-nacre.

[20] Luz GM, Mano JF. Biomimetic design of materials and biomaterials inspired by the structure of nacre. Philos Trans R Soc A: Math Phys Eng Sci 2009;367(1893):1587–605. http://dx.doi.org/10.1098/rsta.2009.0007.

[21] Xie L, Wu K, Liang X, Song Z, Ding J, Jin J, Yao Y, He L, Ni Y. Toughening by interfacial self-healing processes in bioinspired staggered heterostructures. Int J Mech Sci 2025;285:109847. http://dx.doi.org/10.1016/j.ijmecsci.2024.109847.

[22] Abu Bakar IA, Kramer O, Bordas S, Rabczuk T. Optimization of elastic properties and weaving patterns of woven composites. Compos Struct 2013;100:575–91. http://dx.doi.org/10.1016/j.compstruct.2012.12.043, URL https://www.sciencedirect.com/science/article/pii/S0263822313000263.

[23] Lee G, Lee J, Lee S, Rudykh S, Cho H. Extreme resilience and dissipation in heterogeneous elasto-plastomeric crystals. Soft Matter 2024;20:315–29. http://dx.doi.org/10.1039/D3SM01076G.

[24] Chen A, Ezimora U, Lee S, Lee J-H, Gu GX. Sea sponge-inspired designs enhance mechanical properties of tubular lattices. Int J Mech Sci 2025;285:109815. http://dx.doi.org/10.1016/j.ijmecsci.2024.109815.

[25] Gong S, Cui W, Zhang Q, Cao A, Jiang L, Cheng Q. Integrated ternary bioinspired nanocomposites via synergistic toughening of reduced graphene oxide and double-walled carbon nanotubes. ACS Nano 2015;9(12):11568–73. http://dx.doi.org/10.1021/acsnano.5b05252.

[26] Zhang Y, Li Y, Ming P, Zhang Q, Liu T, Jiang L, Cheng Q. Ultrastrong bioinspired graphene-based fibers via synergistic toughening. Adv Mater 2016;28(14):2834–9. http://dx.doi.org/10.1002/adma.201506074.

[27] Das P, Malho J-M, Rahimi K, Schacher FH, Wang B, Demco DE, Walther A. Nacre-mimetics with synthetic nanoclays up to ultrahigh aspect ratios. Nat Commun 2015;6(1):5967. http://dx.doi.org/10.1038/ncomms6967.

[28] Shahzadi K, Mohsin I, Wu L, Ge X, Jiang Y, Li H, et al. Bio-based artificial nacre with excellent mechanical and barrier properties realized by a facile in situ reduction and cross-linking reaction. ACS Nano 2017;11(1):325–34. http://dx.doi.org/10.1021/acsnano.6b05780.

[29] Liu G, Ghosh R, Mousanezhad D, Vaziri A, Nayeb-Hashemi H. Thermal conductivity of biomimetic leaf composite. J Compos Mater 2018;52(13):1737–46. http://dx.doi.org/10.1177/0021998317733316.

[30] Chen W, Zhang P, Yu S, Zang R, Xu L, Wang S, et al. Nacre-inspired underwater superoleophobic films with high transparency and mechanical robustness. Nat Protoc 2022;17(11):2647–67. http://dx.doi.org/10.1038/s41596-022-00725-3.

[31] Xu Z, Wu M, Gao W, Bai H. A sustainable single-component "Silk nacre". Sci Adv 2022;8(19):eabo0946. http://dx.doi.org/10.1126/sciadv.abo0946.

[32] Xiong J, Vaziri A, Ghosh R, Hu H, Ma L, Wu L. Compression behavior and energy absorption of carbon fiber reinforced composite sandwich panels made of three-dimensional honeycomb grid cores. Extrem Mech Lett 2016;7:114–20. http://dx.doi.org/10.1016/j.eml.2016.02.012, URL https://www.sciencedirect.com/science/article/pii/S2352431616300347.

[33] Ghosh R, De S. Z-fiber influence on high speed penetration of 3D orthogonal woven fiber composites. Mech Mater 2014;68:147–63. http://dx.doi.org/10.1016/j.mechmat.2013.06.008, URL https://www.sciencedirect.com/science/article/pii/S0167663613001269.

[34] Levi-Sasson A, meshi I, Mustacchi S, Amarilio I, Benes D, Favorsky V, et al. Experimental determination of linear and nonlinear mechanical properties of laminated soft composite material system. Compos Part B: Eng 2014;57:96–104. http://dx.doi.org/10.1016/j.compositesb.2013.09.043.

[35] Duminy T, Henry R, Adrien J, Doitrand A, Meille S. Anisotropic fracture in nacre-like alumina. Theor Appl Fract Mech 2023;123:103710. http://dx.doi.org/10.1016/j.tafmec.2022.103710, URL https://www.sciencedirect.com/science/article/pii/S0167844222004591.

[36] Currey JD, Taylor JD. The mechanical behaviour of some molluscan hard tissues. J Zool 1974;173(3):395–406. http://dx.doi.org/10.1111/j.1469-7998.1974.tb04122.x.

[37] Currey JD, Sheppard PM. Mechanical properties of mother of pearl in tension. Proc R Soc Lond Ser B. Biological Sci 1977;196(1125):443–63. http://dx.doi.org/10.1098/rspb.1977.0050.

[38] Espinosa HD, Rim JE, Barthelat F, Buehler MJ. Merger of structure and material in nacre and bone – perspectives on de novo biomimetic materials. Prog Mater Sci 2009;54(8):1059–100. http://dx.doi.org/10.1016/j.pmatsci.2009.05.001.

[39] Jackson AP, Vincent JFV, Turner RM, Alexander RM. The mechanical design of nacre. Proc R Soc Lond Ser B. Biological Sci 1988;234(1277):415–40. http://dx.doi.org/10.1098/rspb.1988.0056.

[40] Wang RZ, Suo Z, Evans AG, Yao N, Aksay IA. Deformation mechanisms in nacre. J Mater Res 2001;16(9):2485–93. http://dx.doi.org/10.1557/JMR.2001.0340.

[41] Barthelat F, Tang H, Zavattieri P, Li C-M, Espinosa H. On the mechanics of mother-of-pearl: A key feature in the material hierarchical structure. J Mech Phys Solids 2007;55(2):306–37. http://dx.doi.org/10.1016/j.jmps.2006.07.007.

[42] Menig R, Meyers M, Meyers M, Vecchio K. Quasi-static and dynamic mechanical response of haliotis rufescens (abalone) shells. Acta Mater 2000;48(9):2383–98. http://dx.doi.org/10.1016/S1359-6454(99)00443-7.

[43] Tushtev K, Murck M, Grathwohl G. On the nature of the stiffness of nacre. Mater Sci Eng: C 2008;28(7):1164–72. http://dx.doi.org/10.1016/j.msec.2007.10.039.

[44] Barthelat F. Biomimetics for next generation materials. Philos Trans R Soc A: Math Phys Eng Sci 2007;365(1861):2907–19. http://dx.doi.org/10.1098/rsta.2007.0006.

[45] Li X. Nanoscale structural and mechanical characterization of natural nanocomposites: Seashells. JOM 2007;59(3):71–4. http://dx.doi.org/10.1007/s11837-007-0043-2.

[46] Barthelat F. Designing nacre-like materials for simultaneous stiffness, strength and toughness: Optimum materials, composition, microstructure and size. J Mech Phys Solids 2014;73:22–37. http://dx.doi.org/10.1016/j.jmps.2014.08.008, URL https://www.sciencedirect.com/science/article/pii/S0022509614001756.

[47] Mayer G. New toughening concepts for ceramic composites from rigid natural materials. J Mech Behav Biomed Mater 2011;4(5):670–81. http://dx.doi.org/10.1016/j.jmbbm.2010.08.001, Special Issue on Natural Materials / Papers from the Third International Conference on the Mechanics of Biomaterials and Tissues URL https://www.sciencedirect.com/science/article/pii/S1751616110001086.

[48] Zhang Z, Long Y, Yang Z, Fu K, Li Y. An investigation into printing pressure of 3D printed continuous carbon fiber reinforced composites. Compos Part A: Appl Sci Manuf 2022;162:107162. http://dx.doi.org/10.1016/j.compositesa.2022.107162.

[49] Flores-Johnson E, Shen L, Guiamatsia I, Nguyen GD. A numerical study of bioinspired nacre-like composite plates under blast loading. Compos Struct 2015;126:329–36. http://dx.doi.org/10.1016/j.compstruct.2015.02.083, URL https://www.sciencedirect.com/science/article/pii/S0263822315001725.

[50] Abid N, Pro JW, Barthelat F. Fracture mechanics of nacre-like materials using discrete-element models: Effects of microstructure, interfaces and randomness. J Mech Phys Solids 2019;124:350–65. http://dx.doi.org/10.1016/j.jmps.2018.10.012, URL https://www.sciencedirect.com/science/article/pii/S0022509618303430.

[51] Poloni E, Bouville F, Dreimol CH, Niebel TP, Weber T, Biedermann AR, et al. Tough metal-ceramic composites with multifunctional nacre-like architecture. Sci Rep 2021;11:1621. http://dx.doi.org/10.1038/s41598-021-81068-z.

[52] Slesarenko V, Volokh KY, Aboudi J, Rudykh S. Understanding the strength of bioinspired soft composites. Int J Mech Sci 2017;131–132:171–8. http://dx.doi.org/10.1016/j.ijmecsci.2017.06.054.

[53] Volokh K. Hyperelasticity with softening for modeling materials failure. J Mech Phys Solids 2007;55(10):2237–64. http://dx.doi.org/10.1016/j.jmps.2007.02.012.

[54] Volokh K. On modeling failure of rubber-like materials. Mech Res Commun 2010;37(8):684–9. http://dx.doi.org/10.1016/j.mechrescom.2010.10.006.

[55] Volokh K. New approaches to modeling failure and fracture of rubberlike materials. Adv Polym Sci 2021;286:131–51. http://dx.doi.org/10.1007/12_2020_64.

[56] Slesarenko V, Kazarinov N, Rudykh S. Distinct failure modes in bio-inspired 3D-printed staggered composites under non-aligned loadings. Smart Mater Struct 2017;26(3):035053. http://dx.doi.org/10.1088/1361-665X/aa59eb.

[57] Nairn J, Mendels D. On the use of planar shear-lag methods for stress-transfer analysis of multilayered composites. Mech Mater 2001;33(6):335–62. http://dx.doi.org/10.1016/S0167-6636(01)00056-4.

[58] Weerasinghe A, Lu C-T, Maroudas D, Ramasubramaniam A. Multiscale shear-lag analysis of stiffness enhancement in polymer–graphene nanocomposites. ACS Appl Mater & Interfaces 2017;9(27):23092–8. http://dx.doi.org/10.1021/acsami.7b03159.

[59] Gao X-L, Li K. A shear-lag model for carbon nanotube-reinforced polymer composites. Int J Solids Struct 2005;42(5):1649–67. http://dx.doi.org/10.1016/j.ijsolstr.2004.08.020.

[60] Cong C, Wei Y, Wei X. Trans-scale dynamic shear-lag model for wave attenuation in staggered composites. Int J Mech Sci 2023;238:107841. http://dx.doi.org/10.1016/j.ijmecsci.2022.107841.

[61] Liu C, Shi D, Zhang B, Yang X, Chen H. A novel creep-fatigue life evaluation method for ceramic-composites components. Int J Mech Sci 2023;249:108259. http://dx.doi.org/10.1016/j.ijmecsci.2023.108259, URL https://www.sciencedirect.com/science/article/pii/S0020740323001613.

[62] Han Y, Yong H, Zhou Y. A multi-scale mechanical model of multilevel helical structures with filament damage. Int J Mech Sci 2024;283:109654. http://dx.doi.org/10.1016/j.ijmecsci.2024.109654.

[63] Bao Q, Cui S, Yang Z, Lu Z, He X. Load transfer mechanisms in the platelets reinforced composites with considering the interphase related failure modes. Int J Mech Sci 2023;239:107888. http://dx.doi.org/10.1016/j.ijmecsci.2022.107888.

[64] Bao Q, Yang Z, Lu Z. An improved pull-out model for the composites with curved reinforcement. Int J Mech Sci 2024;262:108733. http://dx.doi.org/10.1016/j.ijmecsci.2023.108733.

[65] Scheuring BM, Christ N, Blarr J, Liebig WV, Hohe J, Montesano J, et al. Experimental and homogenized orientation-dependent properties of hybrid long fiber-reinforced thermoplastics. Int J Mech Sci 2024;280:109470. http://dx.doi.org/10.1016/j.ijmecsci.2024.109470.

[66] Kotha S, Kotha S, Guzelsu N. A shear-lag model to account for interaction effects between inclusions in composites reinforced with rectangular platelets. Compos Sci Technol 2000;60(11):2147–58. http://dx.doi.org/10.1016/S0266-3538(00)00114-7.

[67] Jackson A, Vincent J, Turner R. A physical model of nacre. Compos Sci Technol 1989;36(3):255–66. http://dx.doi.org/10.1016/0266-3538(89)90024-9.

[68] Ji B, Gao H. Mechanical properties of nanostructure of biological materials. J Mech Phys Solids 2004;52(9):1963–90. http://dx.doi.org/10.1016/j.jmps.2004.03.006.

[69] Jin L, Yeager M, Lee Y-J, O'Brien DJ, Yang S. Shape-morphing into 3D curved surfaces with nacre-like composite architectures. Sci Adv 2022;8(41). http://dx.doi.org/10.1126/sciadv.abq3248.

[70] Wang Z, Sheng H, Lin X, Rao Y, Liu J, Lu N. A shear-lag model for laminated beams with extreme modulus mismatch between layers. Mech Mater 2024;188:104844. http://dx.doi.org/10.1016/j.mechmat.2023.104844.

[71] Chen Y, Liu H, Pang K, Zhang C, Qin H, Xu Z, et al. Bending deformable tension-shear model for nacre-like composites. J Mech Phys Solids 2023;171:105132. http://dx.doi.org/10.1016/j.jmps.2022.105132.

[72] Padawer GE, Beecher N. On the strength and stiffness of planar reinforced plastic resins. Polym Eng Sci 1970;l0:185–92.

[73] Liu N, Li S, Wang X. Mechanism of coupling polymer thickness and interfacial interactions on strength and toughness of non-covalent nacre-inspired graphene nanocomposites. Compos Sci Technol 2023;241:110124. http://dx.doi.org/10.1016/j.compscitech.2023.110124, URL https://www.sciencedirect.com/science/article/pii/S0266353823002178.

[74] Mo J, Leung N, Jargalsaikhan U, Wan H, Zhu B, Su B, Sui T. Advanced microscopic characterisation of multi-scale high-resolution mechanical behaviour of a nacre-inspired composite. Compos Commun 2022;35:101315. http://dx.doi.org/10.1016/j.coco.2022.101315, URL https://www.sciencedirect.com/science/article/pii/S2452213922002571.

[75] Grossman M, Pivovarov D, Bouville F, Dransfeld C, Masania K, Studart AR. Hierarchical toughening of nacre-like composites. Adv Funct Mater 2019;29(9):1806800. http://dx.doi.org/10.1002/adfm.201806800.

[76] Liu J, Zhu W, Yu Z, Wei X. Dynamic shear-lag model for understanding the role of matrix in energy dissipation in fiber-reinforced composites. Acta Biomater 2018;74:270–9. http://dx.doi.org/10.1016/j.actbio.2018.04.031, URL https://www.sciencedirect.com/science/article/pii/S1742706118302344.

[77] Cui S, Lu Z, Yang Z, He X. Numerical investigation on the enhanced damping behavior of bio-inspired nacreous composites by introducing interlocked structure. J Mech Behav Biomed Mater 2021;119:104442. http://dx.doi.org/10.1016/j.jmbbm.2021.104442, URL https://www.sciencedirect.com/science/article/pii/S1751616121001296.

[78] Askarinejad S, Shalchy F, Rahbar N. Role of interphase layers in mechanical properties of nacreous structures. Compos Part B: Eng 2021;225:109255. http://dx.doi.org/10.1016/j.compositesb.2021.109255, URL https://www.sciencedirect.com/science/article/pii/S1359836821006314.

[79] Zhang W, Xu J, Yu T. Dynamic behaviors of bio-inspired structures: Design, mechanisms, and models. Eng Struct 2022;265:114490. http://dx.doi.org/10.1016/j.engstruct.2022.114490, URL https://www.sciencedirect.com/science/article/pii/S0141029622005983.

[80] Cilento F, Martone A, Pastore Carbone MG, Galiotis C, Giordano M. Nacre-like GNP/Epoxy composites: Reinforcement efficiency vis-à-vis graphene content. Compos Sci Technol 2021;211:108873. http://dx.doi.org/10.1016/j.compscitech.2021.108873, URL https://www.sciencedirect.com/science/article/pii/S0266353821002293.

[81] Yu Z, Yan Y, Peng Z, Yao Y, Chen S. The selection mechanism of mineral bridges at the interface of stacked biological materials for a strength-toughness tradeoff. J Mech Phys Solids 2024;191:105785. http://dx.doi.org/10.1016/j.jmps.2024.105785, URL https://www.sciencedirect.com/science/article/pii/S0022509624002515.

[82] Liang L, Berto F, Gao C. Silk-inspired architectured filament with enhanced stiffness and toughness for fused deposition modelling (FDM). Compos Part B: Eng 2024;280:111474. http://dx.doi.org/10.1016/j.compositesb.2024.111474, URL https://www.sciencedirect.com/science/article/pii/S1359836824002853.

[83] Patadiya J, Sreenivasan S, Yadav R, Naebe M, Kandasubramanian B. Harnessing fly ash as particle reinforcement in nature-inspired multilayer composites. J Micro Nano Sci Eng 2024;12(1):011002. http://dx.doi.org/10.1115/1.4065964.

[84] Yan Y, Zhao Z-L, Feng X-Q, Gao H. Nacre's brick–mortar structure suppresses the adverse effect of microstructural randomness. J Mech Phys Solids 2022;159:104769. http://dx.doi.org/10.1016/j.jmps.2021.104769, URL https://www.sciencedirect.com/science/article/pii/S002250962100363X.

[85] Nie Y, Li D, Luo Qa. Fracture toughness analysis of interlocked brick and mortar structure considering the anisotropic behavior. Arch Appl Mech 2023;93:2389–409. http://dx.doi.org/10.1007/s00419-023-02387-3.

[86] Zhang Q, Li H, Liu Y, Zhang Z, Yuan Y. Nacre-inspired topological design tuning the impact resistant behaviors of composite plates. Compos Struct 2022;299:116077. http://dx.doi.org/10.1016/j.compstruct.2022.116077.

[87] Abu-Qbeitah S, Petrenko O, Ciavarella M, Rudykh S. Experimental testing of V notched radially graded materials under static loading. Mech Mater 2025;207:105364. http://dx.doi.org/10.1016/j.mechmat.2025.105364, URL https://www.sciencedirect.com/science/article/pii/S0167663625001267.

[88] Wu Y, Fang J, Wu C, Li C, Sun G, Li Q. Additively manufactured materials and structures: A state-of-the-art review on their mechanical characteristics and energy absorption. Int J Mech Sci 2023;246:108102. http://dx.doi.org/10.1016/j.ijmecsci.2023.108102.

[89] Liao B, Yang H, Ye B, Xi L. Microscopic void distribution of 3D printed polymer composites with different printing direction. Mater Lett 2023;341:134236. http://dx.doi.org/10.1016/j.matlet.2023.134236.

[90] Zhang Y, Huang F, Zhang E, Zhang L. Effect of the support bath on embedded 3D printing of soft elastomeric composites. Mater Lett 2023;331:133475. http://dx.doi.org/10.1016/j.matlet.2022.133475.

[91] Chen Y, He Q. 3D-printed short carbon fibre reinforced perforated structures with negative Poisson's ratios: Mechanisms and design. Compos Struct 2020;236:111859. http://dx.doi.org/10.1016/j.compstruct.2020.111859.

[92] Ning F, Cong W, Qiu J, Wei J, Wang S. Additive manufacturing of carbon fiber reinforced thermoplastic composites using fused deposition modeling. Compos Part B: Eng 2015;80:369–78. http://dx.doi.org/10.1016/j.compositesb.2015.06.013.

[93] Russ J, Slesarenko V, Rudykh S, Waisman H. Rupture of 3D-printed hyperelastic composites: Experiments and phase field fracture modeling. J Mech Phys Solids 2020;140:103941. http://dx.doi.org/10.1016/j.jmps.2020.103941, URL https://www.sciencedirect.com/science/article/pii/S0022509620301770.

[94] San B, Waisman H. Optimization of carbon black polymer composite microstructure for rupture resistance. J Appl Mech 2016;84(2):021005. http://dx.doi.org/10.1115/1.4035050.

[95] Lian K, Yang L, Zhu D, Gong X, Zhang H, Wang K, Li J, Yu W. Effect of printing parameters on 3D-printed carbon fiber-reinforced polymer composites under magnetic field control. J Manuf Process 2023;101:1443–52. http://dx.doi.org/10.1016/j.jmapro.2023.07.040.

[96] Rimašauskas M, Jasiūnienė E, Kuncius T, Rimašauskienė R, Cicėnas V. Investigation of influence of printing parameters on the quality of 3D printed composite structures. Compos Struct 2022;281:115061. http://dx.doi.org/10.1016/j.compstruct.2021.115061.

[97] Stratasys. Performance properties URL https://www.stratasys.com/en/materials/materials-catalog/polyjet-materials/.

[98] Zhang X, Wu K, Ni Y, He L. Anomalous inapplicability of nacre-like architectures as impact-resistant templates in a wide range of impact velocities. Nat Commun 2022;13(1):7719. http://dx.doi.org/10.1038/s41467-022-35439-3.

[99] Slesarenko V, Rudykh S. Harnessing viscoelasticity and instabilities for tuning wavy patterns in soft layered composites. Soft Matter 2016;12:3677–82. http://dx.doi.org/10.1039/C5SM02949J.

[100] Chintapalli RK, Breton S, Dastjerdi AK, Barthelat F. Strain rate hardening: A hidden but critical mechanism for biological composites? Acta Biomater 2014;10(12):5064–73. http://dx.doi.org/10.1016/j.actbio.2014.08.027.

[101] Slesarenko V, Rudykh S. Towards mechanical characterization of soft digital materials for multimaterial 3D-printing. Internat J Engrg Sci 2018;123:62–72. http://dx.doi.org/10.1016/j.ijengsci.2017.11.011.